

## Fouling mechanisms of *Pseudomonas putida* on PES microfiltration membranes

Irene Rosas, Sergio Collado, Antonio Gutiérrez, Mario Díaz

Department of Chemical Engineering and Environmental Technology, University of Oviedo, c/  
Julian Claveria, s/n Oviedo, 33071 Oviedo, Spain

### Abstract

The mechanisms by which *Pseudomonas putida* causes fouling on a microfiltration membrane have been studied. For an initial *P. putida* concentration of 0.77 g/L ( $5.1 \times 10^8$  cfu/mL) stirred dead-end tests indicated that approximately 70% of the permeability was lost during the first minute of filtration and only 15% more was lost during the following 24 min. SEM observations showed the presence of aggregates within the most external part of the membrane pores, partially blocking these pores and leading to more or less regular surface deposits and consequently, an intermediate blocking model was proposed and successfully fitted. The analysis of fouling resistance-in-series indicated that the selection of a high TMP during the microfiltration of *P. putida* had no effect on the final permeate flux but provoked an increase in external in comparison to internal fouling. On the other hand, the selection of a lower TMP led to a low rate of accumulation of *P. putida* on the membrane, reducing the total membrane resistance and allowing a deeper penetration of the bacteria into the pore. Studies on the cleanability of the membrane using sonication showed how this technique was more effective when membrane was fouled at higher TMP, achieving permeability recoveries of around 80% in the best cases.

### Keywords

Fouling, Microfiltration, PES membrane, *P. putida*, Stirred dead-end

### 1. Introduction

*Pseudomonas putida* is a rod-shaped, Gram-negative, bacterium that is very common in soil and freshwater environments. It plays a very important role in the decomposition that drives the carbon cycle because it can break down all manner of aliphatic and aromatic hydrocarbons. This ability of *P. putida* to grow on several aromatic hydrocarbon compounds has a direct bearing on the development of strategies for dealing with environmental pollution [1].

For this reason, *P. putida* has become a versatile environmental isolate that has been widely utilized to remove a wide range of recalcitrant pollutants in water and soil, aiming at the complete degradation of these compounds into carbon dioxide and water. Treatments employed involve the use of pure cultures of *P. putida* or their addition to mixed microbial populations for the depuration of soils, wastewaters, natural waterways, aquifers, etc. [2], [3], [4], [5], [6].

The use of *P. putida* for the removal of pollutants during wastewater treatment requires different processes for the retention of the cells and their separation from the final effluent. Although cell immobilization is now a relatively well-established technique, a suspended cellular suspension is frequently preferred [2], [7], [8], [9] for wastewater treatment due to its simplicity and lower cost. In this case, a physical separation process is necessary in order to obtain a higher cell density in the bioreactor and a final effluent without suspended solids. Membrane separation processes, particularly microfiltration and ultrafiltration, are mature commercial

technologies that are frequently applied for biomass retention [10], [11], [12]. Given that membrane fouling is the major obstacle to the broader application of microfiltration (MF) and ultrafiltration (UF) to water and wastewater treatment, it is not surprising that the majority of research into membrane materials and processes and their development is devoted to the characterization and amelioration of this important problem [13], [14]. Membrane fouling can be divided into three kinds according to the nature of the foulants: inorganic fouling (e.g. scaling), organic fouling (e.g. proteins, humic substances, etc.) and biofouling (e.g. deposition of microorganisms) [15]. In contrast to inorganic and organic fouling, which can be controlled easily and removed by physical and chemical cleaning, removal of biofouling is more complex as microorganisms can adhere to the membrane surface and multiply [16].

In this regard, one of the most significant problems limiting membrane biofouling control is the inadequate understanding of the basic mechanisms governing adsorption/deposition of foulants in and on membranes and, to the best of our knowledge, there has been little research into membrane biofouling caused by *P. putida*. In fact, only two previous contributions have been found in the bibliography, the first of which studies the growth behavior of *P. putida* on a 0.22  $\mu\text{m}$  mixed cellulose esters (MCE) membrane [17], while the second, carried out by the authors, focuses on fouling in pleated membrane cartridges [18]. However, no previous works were found on membrane fouling caused by *P. putida* filtration with PES membranes, even though this polymer is widely used as a membrane material. More detailed knowledge of the characteristics and development of fouling caused by *P. putida* on PES membranes could contribute to the improvement of the biotreatment process of phenolic compounds.

Based on these considerations, the aim of this work is to investigate the characteristics of the fouling of a PES membrane during stirred dead end microfiltration, with a culture of *P. putida*, elucidating the different fouling mechanisms involved.

## 2. Materials and methods

### 2.1. Microorganism and culture conditions

Microfiltration experiments were carried out with a culture of *P. putida* DSM 4478 (German Resource Centre for Biological Material) which was selected for its capacity for degrading salicylic acid. Cell suspensions were collected from a bioreactor of 20 L capacity for carrying out the degradation of salicylic acid. The synthetic wastewater used in this study mainly consisted of mineral salt medium (MSM) whose composition was (g/L)  $\text{KH}_2\text{PO}_4$  (0.422),  $\text{K}_2\text{HPO}_4$  (0.375),  $(\text{NH}_4)_2\text{SO}_4$  (0.244),  $\text{MgSO}_4 \cdot 7\text{H}_2\text{O}$  (0.05),  $\text{NH}_3 \cdot \text{Fe} \cdot \text{Citrate}$  (0.054), NaCl (0.015),  $\text{CaCl}_2 \cdot 12\text{H}_2\text{O}$  (0.015) and tryptone 0.05, supplemented with salicylic acid as the sole carbon source.

Cell concentrations were estimated by correlating OD at 600 nm with dry cell weight or with cells/mL. One OD unit is equivalent to a dry weight of 0.45 g/L or to a cellular viability of  $3.0 \times 10^8$  cfu/mL. At the time of carrying out the stirred dead end experiments, the *P. putida* concentration was 0.77 g/L or  $3.3 \times 10^8$  cfu/mL. Measurements were made at least in duplicate. The standard deviation was found to be below 5% in all cases.

### 2.2. Stirred dead-end microfiltration module and membranes

In order to evaluate the filterability of cellular suspension and its supernatant, microfiltration experiments were conducted using a stirred dead-end microfiltration module (Fig. 1) (Model 8200, Cat. no. 5123) with an effective membrane surface area of  $2.87 \times 10^{-3}$  m<sup>2</sup>. A volume of 100 mL of cellular suspension or its supernatant was filtered. The bacteria are still alive during

the filtration experiments. The stirring speed was adjusted to 300 rpm. Experiments carried out by Zokae et al. [19] suggest that the stirring speed influences the decrease in concentration polarization while others such as Lim and Bai [20] suggest that the mechanism of fouling by concentration polarization may be negligible in microfiltration, due to the increased size of retained particles. In this paper, the stirring speed is used to maintain a uniform concentration in the suspension during the whole process, avoiding sedimentation of particles. Also, according to Wang [21], under constant pressure and suspension concentration, specific cake resistance is independent of agitation velocity. The operating pressure is supplied by compressed air, working at two different constant pressures: 20 kPa and 50 kPa.

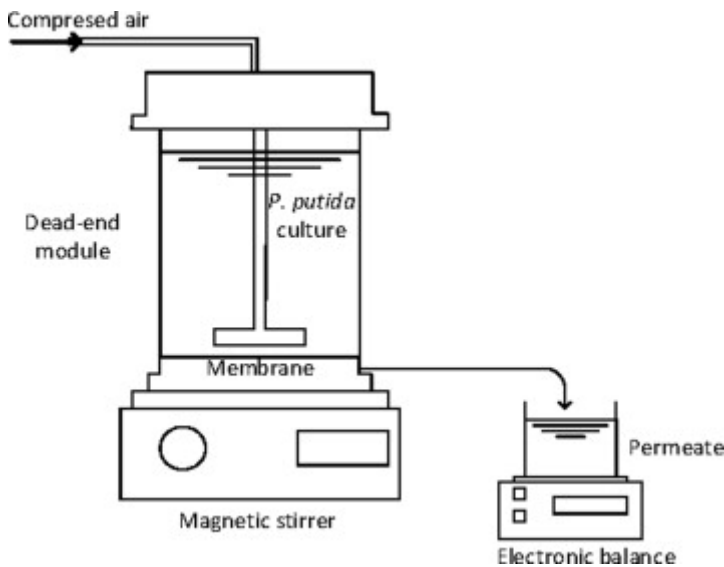


Fig. 1. Diagram of stirred dead-end microfiltration module.

Polyethersulfone membranes (PES) (Cat. no. GPWP09050) were acquired from Millipore Corporation. Membrane characteristics are listed in Table 1. The membrane had a sponge-like microstructure with interconnected pore morphology. This membrane material was selected because it is one of the polymers most frequently employed in the water industry, with high chemical resistance and mechanical strength [22].

Table 1. Membrane characteristics.

<b>Material</b>	PES
<b>Pore size (<math>\mu\text{m}</math>)</b>	0.22
<b>Porosity (%)</b>	75
<b>Hydrophilic</b>	Yes
<b>Surface</b>	Plain
<b>Thickness (<math>\mu\text{m}</math>)</b>	$\geq 160$ and $\leq 185$

### 2.3. Membrane cleaning by sonication

In order to investigate the effectiveness of sonication as a cleaning method, membranes were submerged in ultrapure water in an ultrasound bath (Ultrasounds, P Selecta) at 360 W for 5 min at room temperature. After the sonication cycle, pure water flux was measured by three measurements of flux in the pressure range 50–200 kPa.

## 2.4. Scanning electron microscopic (SEM) images

The surfaces of the fresh, fouled and cleaned membranes were analyzed by scanning electron microscopy using a JEOL-6100 scanning electron microscope (JEOL Ltd., Tokyo, Japan). Fresh membranes were dried in an oven during 24 h to ensure that they were completely dry. When dry, membranes were mounted on aluminum stubs with double-sided carbon sticky tape, sputtered with gold in a vacuum evaporator (Balzers SCD 004, BAL-TEC AG), prior to observation under the SEM.

## 3. Results and discussion

### 3.1. Suspension microfiltration of *P. putida*

In order to elucidate the characteristics of fouling on the PES membrane due to *P. putida*, a volume of 100 mL of cellular suspension was filtered for 25 min under two constant transmembrane pressures: 20 and 50 kPa. The sampling time interval was fixed at 30 s. Fig. 2 shows the permeability of the membrane suspension at the two pressures.

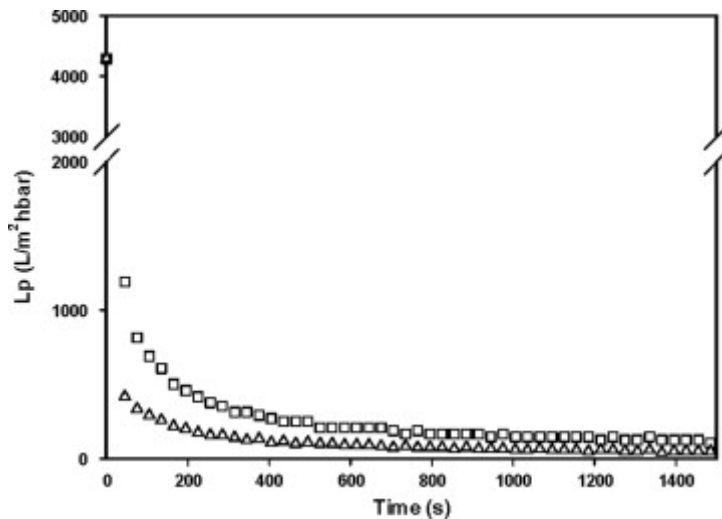


Fig. 2. Membrane permeability versus time for two TMP: 20 kPa ( $\square$ ) and 50 kPa ( $\Delta$ ). Broken line denotes initial water permeability of the membrane. In both cases:  $T=301$  K, initial *P. putida* concentration: 0.77 g/L ( $5.1 \times 10^8$  cfu/mL).

The initial water permeability of the membrane is  $4290 \text{ L/m}^2 \text{ h bar}$ . For both assayed TMPs, the permeability decreased rapidly during the experiment, finally reaching values of around 100 and 50  $\text{L/m}^2 \text{ h bar}$  for 0.2 bar and 0.5 bar, respectively, after 25 min of filtration. These results indicate that there are reductions in permeability at the end of the experiment of around 97.6% and 98.8%. These observations correspond to typical permeability variations encountered in stirred dead-end MF at constant TMP. As shown in the figure, the permeability decline was not linear with time. For example, around 70% of the permeability was lost during the first minute and only 15% more was lost during the following minutes. According to several authors, this drastic flux decline, observed during the first minute of filtration, may be due to the fast accumulation on the membrane surface of a first layer of fouling, which is thin but very resistant to mass transfer due to its low porosity. After that, the structure of the newly formed layers is less compact, indicating the existence of a porosity gradient through the cake thickness [8], [23], [24].

It can be seen in Fig. 2 that the reduction in permeability was faster when a higher TMP was selected, indicating a higher accumulation of foulants on the membrane surface and/or that these foulants have a lower porosity. Thus, it can be observed that the permeability of the membrane when the TMP was 0.2 bar is approximately twice that obtained when the selected TMP was 0.5 bar for all the filtration times assayed. In fact, a permeate flux of around  $20 \text{ L m}^{-2} \text{ h}^{-1}$  was obtained at the end of the filtration time for both TMPs. Zokae et al. also observed similar behavior during the microfiltration of concentrated cultures of *Escherichia coli* [19]. It should be recalled that the initial flux is different for each case, since it is proportional to TMP, indicating that the flux at 0.5 bar dropped abruptly, with a reduction of 96.4% after 2 min of filtration, versus the 84.0% reduction observed for a TMP of 0.2 bar.

Pressure independence of the flux indicates a mass-transfer controlled filtration, that is, the rate of membrane filtration under the conditions of TMP and *P. putida* concentration is controlled by the rate at which retained material is transported from the membrane back into the bulk fluid. Accordingly, operating strategies that assist back-transport of concentrated solutes, such as using faster fluid flow rates, stirring the feed material, or increasing the temperature, are generally successful in improving filtration. In order to determine the concentration of *P. putida* below which pressure-driven microfiltration is predominant, Fig. 3 shows the evolution of permeability against the concentration of bacteria in the retentate ( $X$ ), which can be calculated as

$$X = \frac{V_0 X_0}{(V_0 - V_F)} \quad (1)$$

where  $V_0$  and  $X_0$  are the initial volume of medium (0.1 L) and *P. putida* concentration, respectively, and  $V_F$  is the cumulative filtered volume.

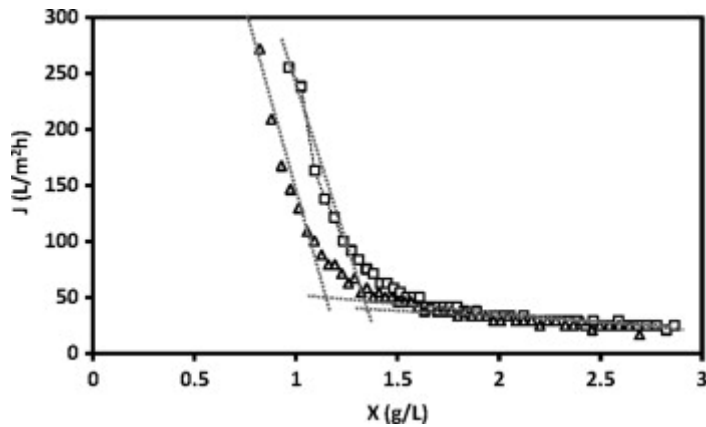


Fig. 3. Membrane permeability versus concentration of *P. putida* in the retentate for two TMP: 0.2 bar (□) and 0.5 bar (Δ). Broken line denotes initial water permeability of the membrane. In both cases:  $T=301 \text{ K}$ , initial *P. putida* concentration:  $0.77 \text{ g/L}$  ( $5.1 \times 10^8 \text{ cfu/mL}$ ).

Two steps can be distinguished in Fig. 3: initially, the permeability declined rapidly when the bacterial concentration increased and then was practically independent of concentration. So, in the second stage, a more or less constant flux of around  $20 \text{ L/m}^2 \text{ h}$  for 0.2 and 0.5 TMP is reached, as has previously been indicated. The transition between these steps defines the limiting concentration between pressure and mass-transfer controlled regions [25]. For TMP of 0.2 bar and 0.5 bar, these concentrations were around  $1.4 \text{ g/L}$  ( $9.3 \times 10^8 \text{ cfu/mL}$ ) and  $1.0 \text{ g/L}$  ( $6.7 \times 10^8 \text{ cfu/mL}$ ), respectively. These data are in agreement with the fact that pressure-driven

microfiltration occurs at low TMP and concentration of bacteria, whereas mass-controlled microfiltration is favored by high TMP and bacterial concentration.

Additionally, a volume of 100 mL of supernatant, which was obtained from the cellular suspension by centrifugation, was also filtered. However, no significant loss of permeability was observed in this case, indicating that fouling is mainly due to the bacteria in suspension.

### 3.2. Analysis of fouling resistances

The permeation flux through a microfiltration unit treating suspensions, such as activated sludge wastewater can be given as:

$$J = \frac{\Delta P}{\mu(R_M + R_{ef} + R_{if})} \quad (2)$$

where  $R_M$  is the intrinsic membrane resistance,  $R_{ef}$  is the external fouling resistance formed by a strongly deposited fouling layer from physico-chemical interactions of solids with the membrane surface and  $R_{if}$  is the internal fouling resistance due to some irreversible adsorption [26], [27].  $R_M$  is estimated by measuring the tap water flux for new membrane ( $J_w$ ):

$$R_M = \frac{TMP}{\mu_w J_w} \quad (3)$$

where  $\mu_w$  is the viscosity of fresh water. Because the external fouling can be washed off by water flushing, while internal fouling would remain unchanged, thus,  $R_{if}$  can be estimated according to tap water flux through the cleaned mesh ( $J'_w$ ) as [28]

$$R_{if} = \frac{TMP}{\mu_w J'_w} - R_M \quad (4)$$

Finally, if  $J_s$  is defined as the flux achieved at the end of the microfiltration of *P. putida* culture,  $R_{ef}$  can be calculated as

$$R_{ef} = \frac{TMP}{\mu J_s} - R_{if} - R_M \quad (5)$$

Fig. 4 shows the filtration resistances obtained during the microfiltration of the *P. putida* culture for each transmembrane pressure used. As can be seen, the total resistance of the fouling when the TMP selected was 0.5 bar was approximately two and a half times higher than that obtained for a TMP of 0.2 bar, which was foreseeable because flux decline was more marked at 0.5 bar than at 0.2 bar.

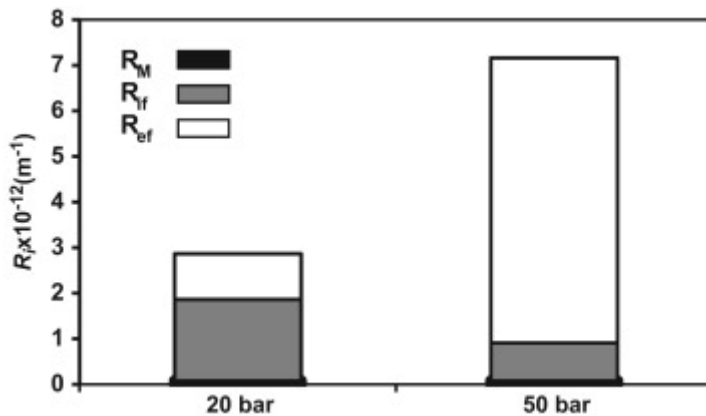






Fig. 4. Fouling resistances obtained for the microfiltration of *P. putida* culture using a PES membrane. In both cases:  $T=301\text{ K}$ , initial *P. putida* concentration:  $0.77\text{ g/L}$  ( $5.1 \times 10^8\text{ cfu/mL}$ ).

Additionally, the fraction of each resistance in the total filtration resistance also changed with the TMP selected. Thus, for 0.5 bar, the internal and external fouling resistances represented 62.3% and 35.0%, of the total resistance respectively. On the other hand, these values for a TMP of 0.2 bar were 11.6% and 87.3% for the internal and external fouling resistances, respectively. In both cases, the contribution of the membrane to the total resistance was negligible ( $R_M < 3\%$ ). Therefore, it can be concluded that the employment of a high TMP during the microfiltration of *P. putida* leads to an increase in external as opposed to internal fouling.

### 3.3. Fouling mechanism

In order to elucidate the fouling mechanism involved in the loss of permeability of the PES membrane during the stirred dead-end microfiltration of *P. putida*, data of permeate volumes versus time of filtration obtained for 0.2 bar and 0.5 bar were fitted using the individual and combined fouling models proposed by Bolton et al. [29]. The best fit was determined by minimizing the sum of squared residuals (SSR) where residual was equal to the difference between a data point and the model prediction. Table 2 shows a brief description of the simple mechanisms of membrane fouling, the fitted parameters of the models and the SRR values for each model while the data and the model fits are compared in Fig. 5.

Table 2. Main mechanisms of fouling: brief description, fitted parameters and SRR obtained using the experimental data. In both cases:  $T=301\text{ K}$ , initial *P. putida* concentration:  $0.77\text{ g/L}$  ( $5.1 \times 10^8\text{ cfu/mL}$ ).

Blocking	Complete	Intermediate	Cake	Standard
Figure				
Description	Particles seal off pore entrances	A portion of the particles seal off pores and the rest accumulate on the top of other deposited particles	Particles accumulate on the surface of the membrane in a permeable cake of increasing thickness	Particles accumulate inside membrane on the walls of straight cylindrical pores
Model	$V = \frac{A_0}{K_b}(1 - e^{-K_b t})$	$V = \frac{A_0}{K_i} \ln(1 + K_i J_0 t)$	$V = \frac{1}{K_c J_0} (\sqrt{1 + 2K_c J_0^2 t} - 1)$	$V = \left(\frac{1}{J_0} + \frac{K_s}{2}\right)^{-1}$
0.2 bar	Fitted parameter $K_b = 3.7 \times 10^{-3} \text{ s}^{-1}$ $r^2 = 0.89$ SRR = $1.8 \times 10^{-4}$	$K_i = 115.5 \text{ m}^{-1}$ $r^2 = 0.998$ SRR = $3.4 \times 10^{-6}$	$K_c = 3,902,863 \text{ s.m}^{-2}$ $r^2 = 0.96$ SRR = $6.0 \times 10^{-5}$	$K_s = 75.1 \text{ m}^{-1}$ $r^2 = 0.97$ SRR = $4.4 \times 10^{-5}$
0.5 bar	Fitted parameter $K_b = 3.4 \times 10^{-3} \text{ s}^{-1}$ $r^2 = 0.91$ SRR = $1.7 \times 10^{-4}$	$K_i = 105.8 \text{ m}^{-1}$ $r^2 = 0.9991$ SRR = $1.7 \times 10^{-6}$	$K_c = 3476217 \text{ s.m}^{-2}$ $r^2 = 0.96$ SRR = $6.3 \times 10^{-5}$	$K_s = 69.8 \text{ m}^{-1}$ $r^2 = 0.98$ SRR = $3.8 \times 10^{-5}$

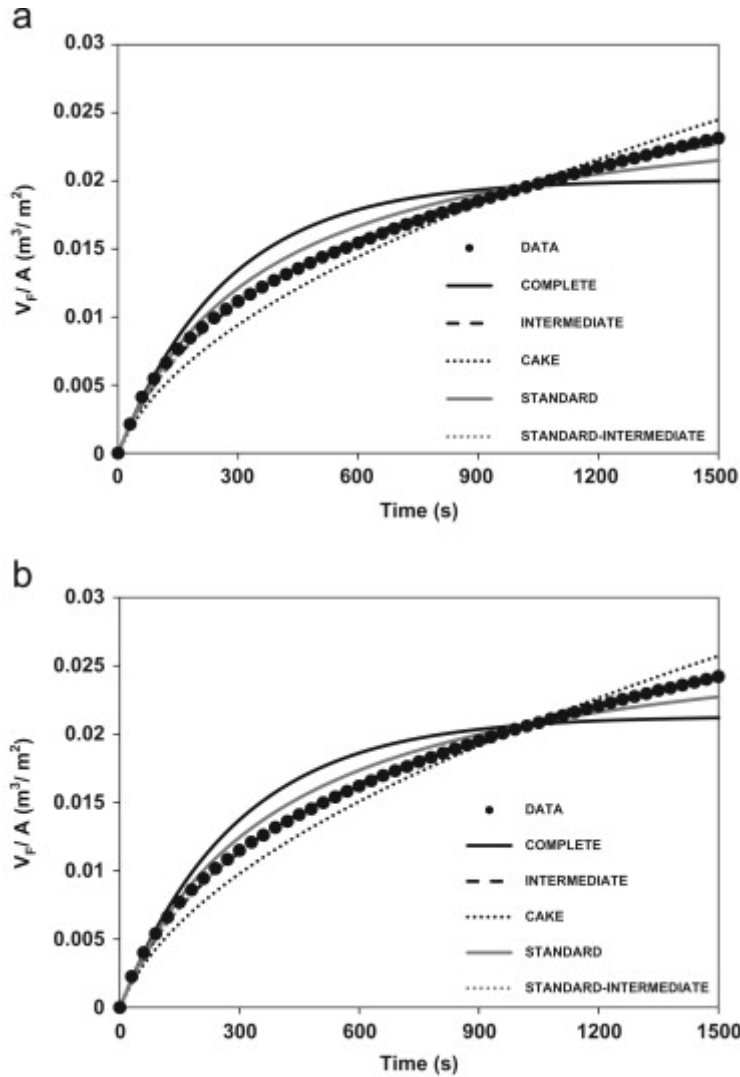


Fig. 5. Volume versus time data compared to the complete model, intermediate model, cake model, standard model and standard-intermediate model predictions for  $\text{TMP} = 0.2$  bar (a) and  $\text{TMP} = 0.5$  bar (b). In both cases:  $T = 301$  K, initial *P. putida* concentration:  $0.77 \text{ g/L}$  ( $5.1 \times 10^8 \text{ cfu/mL}$ ).

For both TMPs, the best fit of the data occurred with the intermediate blocking model, which had an SRR twenty-fold lower than those obtained for the standard blocking model. These results suggest that each bacterium may settle on another particle that has already arrived and is blocking some pores, or it may also directly block an area of membrane. An intermediate



blocking model has also been proposed by several authors as the main fouling mechanism during the stirred dead-end microfiltration of waste water from an activated sludge reclamation plant [30]. In another study, Wendong et al. observed that intermediate pore blocking followed by cake filtration is the governing mechanism in biofouling during microfiltration of fermentation broth [31]. In fact, intermediate pore blocking followed by cake filtration is a common fouling mechanism in many applications, including microfiltration of different wastewaters [32], [33]. In this combined model, it is assumed that intermediate pore blocking proceeds from the beginning of the experiment up to a defined time of operation. After that, solutes start to be deposited on the membrane surface, resulting in cake formation, which eliminates the effect of the blocking phenomena [33]. In our case, the effect of cake formation on the decline in membrane flux was not observed. This can be attributed to two factors. The first is that the cake layer thickness is restricted by the external cross flow caused by the high agitation speed. Stirring induces a tangential or cross flow during the filtration, causing a sweeping effect on the membrane. The second reason is that a higher filtration time could be required for the development of the cake layer.

To better understand how bacterial deposition on the membrane occurs, SEM images of different regions of the fouled membrane were taken to illustrate the deposition patterns of *P. putida* on the membrane surface (Fig. 6).

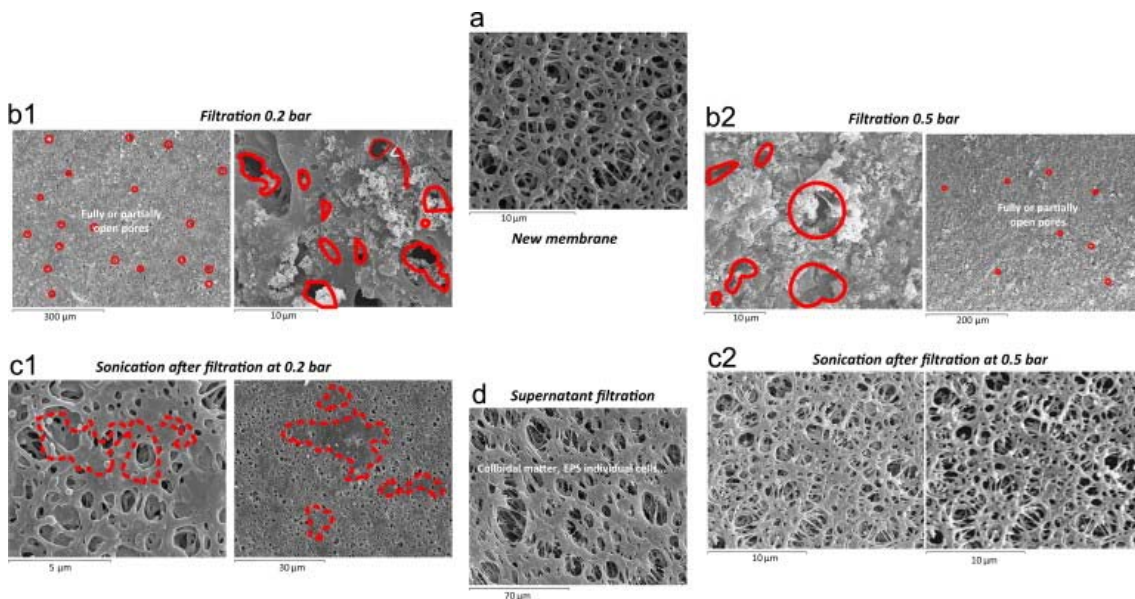


Fig. 6. Scanning electron micrographs of the new membrane (a), the fouled membrane after filtration of a *P. putida* culture (b) or its supernatant (d) and membrane after cleaning using a sonication process (c).

SEM observations showed the presence of aggregates within the most external part of the membrane pores, partially blocking these pores and leading to more or less uniform surface deposits. It should be noted that the obstruction of the pore inlet is not complete. As it can be seen in Fig. 6b1 and b2 (see red lines), a high proportion of the pore entrances is only partially sealed after the filtration. As was mentioned above, an increase in TMP accelerates the rate of fouling (see Fig. 2). When the applied pressure was 0.5 bar, it was expected that the fouling layer would be formed faster than at 0.2 bar, resulting in an accumulation of bacteria in the part of the pores located in the immediate vicinity of the surface. These accumulated bacteria would subsequently act as a filter media for the suspended particles. The selection of a lower TMP involves a low rate of accumulation of fouling, presumably allowing a deeper penetration of the

bacteria into the pore (see Fig. 7). This is also in accordance with the fouling resistances calculated previously. Thus, external as opposed to internal fouling resistance was the main contributor to the total filtration resistance in the microfiltration of *P. putida* culture at 0.5 bar, whereas the opposite behavior was observed when a lower TMP was selected.

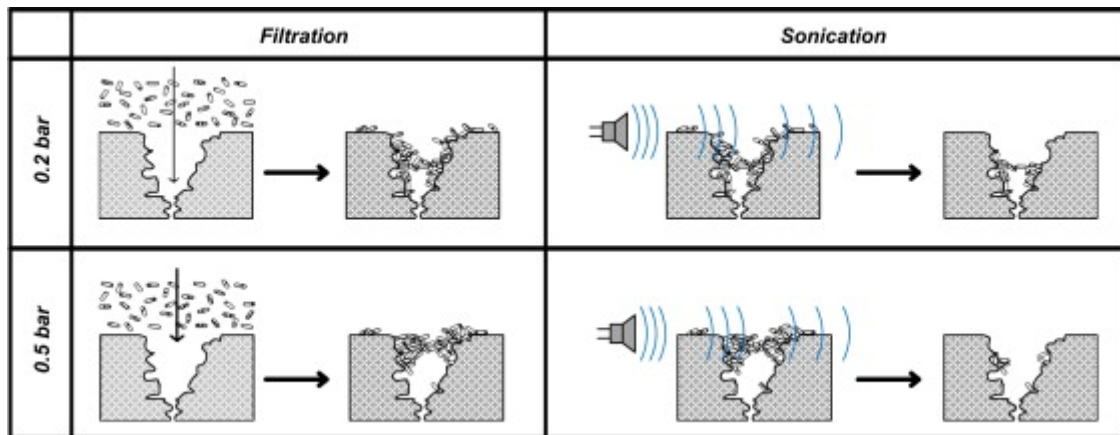


Fig. 7. Schematic representation of the microfiltration of *P. putida* and the subsequent sonication of the fouled membrane.

is also explains why SEM micrographs of the fouled membranes showed the presence of a high number of pores with their entrances partially obstructed by the bacteria; a higher proportion of the pore entrance was obstructed when a higher TMP was selected (Fig. 6b1 and b2). It is also evident that the proportion of completely sealed pores was higher when the TMP increased.

### 3.4. Cleaning

To evaluate the cleanability of the membrane, the membranes fouled with the cellular suspension of *P. putida* at different working pressures, 20 and 50 kPa, were submerged in ultrapure water in an ultrasound bath (Ultrasounds, P Selecta) at 360 W for 5 min at room temperature. Fig. 8 shows the water permeability of the new, fouled and cleaned membrane. Permeability recovery (R) can be defined as

$$R = \frac{L_{P,after\ cleaning} - L_{P,before\ cleaning}}{L_{P, initial}} \times 100 \quad (6)$$

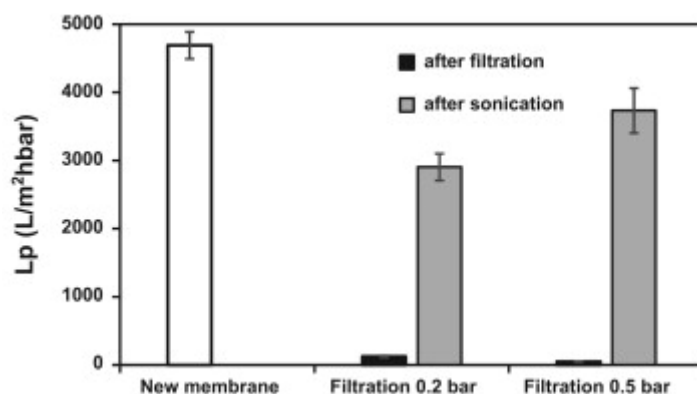


Fig. 8. Permeability of the new membrane (white bar) and the membranes after filtration of the cellular suspension of *P. putida* (black bars) and a subsequent sonication (gray bars).

Results show permeability recoveries of 59.2% for 0.2 bar and 78.2% for 0.5 bar, obtaining final permeabilities after cleaning of 61.9% and 79.6% of the initial value, respectively. It is evident

that sonication was more effective when the membrane was fouled at higher TMP. This is because sonication is not effective in cleaning all types of fouling on the membranes [20], [26]. Certain forms of fouling (particularly when it is inside the pore, that is, internal fouling) were not effectively removed by sonication, whereas this technique is effective in cleaning membranes when the fouling is near to the pore entrance or on the membrane surface (external fouling) (Fig. 7). As was previously explained, a lower TMP during the microfiltration allows a deeper penetration of the bacteria inside the membrane pores, thus making cleaning by means of sonication more difficult and reducing the flux recovery (Fig. 8). This behavior is also consistent with SEM images of the membranes after the sonication (Fig. 6c1 and c2), where some fouled areas can be observed for TMP 0.2 bar, whereas the membrane surface for TMP 0.5 bar was largely free of particles.

#### 4. Conclusions

The fouling caused by *P. putida* cultures on PES microfiltration membranes was studied. Stirred dead-end experiments showed an initial fast decline in the permeability followed by a second step in which permeability remained constant; this state of mass-transfer controlled microfiltration being reached at or above bacterial concentrations of 1–1.5 g/L, that is  $6.7 \times 10^8$ – $9.3 \times 10^8$  cfu/mL. An intermediate blocking model was the prevailing fouling mechanism ( $K_i \approx 110 \text{ m}^{-1}$ ).

Analysis of the resistance-in-series indicated that high TMP causes the rapid formation of a layer of fouling on the external surface of the membrane, whereas low TMP favored the penetration of bacteria into the pore, increasing the degree of internal fouling with respect to that of external fouling. High TMP also had a positive effect on the cleanability of the membrane by means of sonication, with permeability recoveries of around 80% for TMP 0.5 bar, because this technique is more effective when the fouling is near to the pore entrance or on the membrane surface.

#### References

- [1] K.-C. Loh, B. Cao. Paradigm in biodegradation using *Pseudomonas putida*—a review of proteomics studies. *Enzyme and Microbial Technology*, 43 (2008), pp. 1-12.
- [2] X. Ma, N. Li, J. Jiang, Q. Xu, H. Li, L. Wang, J. Lu. Adsorption–synergic biodegradation of high-concentrated phenolic water by *Pseudomonas putida* immobilized on activated carbon fiber. *Journal of Environmental Chemical Engineering*, 1 (2013), pp. 466-472.
- [3] T. Abuhamed, E. Bayraktar, T. Mehmetoğlu, Ü. Mehmetoğlu. Kinetics model for growth of *Pseudomonas putida* F1 during benzene, toluene, and phenol biodegradation. *Process Biochemistry*, 39 (2004), pp. 983-988.
- [4] P.U.M. Raghavan, M. Vivekanandan. Bioremediation of oil-spilled sites through seeding of naturally adapted *Pseudomonas putida*. *International Biodeterioration & Biodegradation*, 44 (1999), pp. 29-32.
- [5] F.-B. Yu, S.W. Ali, L.-B. Guan, S.-P. Li, S. Zhou. Bioaugmentation of a sequencing batch reactor with *Pseudomonas putida* ONBA-17 and its impact on reactor bacterial communities. *Journal of Hazardous Materials*, 176 (2010), pp. 20-26.
- [6] G. Bengtsson, A. Fossum, R. Lindqvist. Persistence of plasmid RP4 in *Pseudomonas putida* and loss of its expression of antibiotic resistance in a groundwater microcosm. *Soil Biology and Biochemistry*, 36 (2004), pp. 999-1008.
- [7] M.H. El-Naas, A.-H.I. Mourad, R. Surkatti. Evaluation of the characteristics of polyvinyl alcohol (PVA) as matrices for the immobilization of *Pseudomonas putida*. *International Biodeterioration & Biodegradation*, 85 (2013), pp. 413-420.

- [8] J. Mendret, C. Guigui, P. Schmitz, C. Cabassud. In situ dynamic characterization of fouling under different pressure conditions during dead-end filtration: compressibility properties of particle cakes. *Journal of Membrane Science*, 333 (2009), pp. 20-29.
- [9] I. Banerjee, J.M. Modak, K. Bandopadhyay, D. Das, B.R. Maiti. Mathematical model for evaluation of mass transfer limitations in phenol biodegradation by immobilized *Pseudomonas putida*. *Journal of Biotechnology*, 87 (2001), pp. 211-223.
- [10] A. Fenu, G. Guglielmi, J. Jimenez, M. Spèrandio, D. Saroj, B. Lesjean, C. Brepols, C. Thoeye, I. Nopens. Activated sludge model (ASM) based modeling of membrane bioreactor (MBR) processes: a critical review with special regard to MBR specificities. *Water Research*, 44 (2010), pp. 4272-4294.
- [11] A. Fenu, J. Roels, T. Wambecq, K. De Gussem, C. Thoeye, G. De Guedre, B. Van De Steene. Energy audit of a full-scale MBR system. *Desalination*, 262 (2010), pp. 121-128.
- [12] J. Hoinkis, S.A. Deowan, V. Panten, A. Figoli, R.R. Huang, E. Drioli. Membrane Bioreactor (MBR) technology—a promising approach for industrial water reuse. *Procedia Engineering*, 33 (2012), pp. 234-241.
- [13] A. Pollice, A. Brookes, B. Jefferson, S. Judd. Sub-critical flux fouling in membrane bioreactors—a review of recent literature. *Desalination*, 174 (2005), pp. 221-230.
- [14] T. Zsiri, P. Buzatu, P. Aerts, S. Judd. Efficacy of relaxation, backflushing, chemical cleaning, and clogging removal for an immersed hollow fiber membrane bioreactor. *Water Research*, 46 (2012), pp. 4499-4507.
- [15] P. Le-Clech, V. Chen, T.A.G. Fane. Fouling in membrane bioreactors used in wastewater treatment. *Journal of Membrane Science*, 284 (2006), pp. 17-53.
- [16] H.C. Flemming. Biofouling in water systems—cases, causes and countermeasures. *Applied Microbiology and Biotechnology*, 59 (2002), pp. 629-640.
- [17] Y. Chao, T. Zhang. Growth behaviors of bacteria in biofouling cake layer in a dead-end microfiltration system. *Bioresource Technology*, 102 (2011), pp. 1549-1555.
- [18] I. Rosas, S. Collado, I. Fernández, A. Gutierrez-Lavin, M. Diaz. Fouling in pleated microfiltration cartridges caused by *Pseudomonas putida*. *Journal of Membrane Science*, 443 (2013), pp. 107-114.
- [19] F. Zokaee, T. Kaghazchi, A. Zare. Cell harvesting by microfiltration in a dead-end system. *Process Biochemistry*, 34 (1999), pp. 803-810.
- [20] A.L. Lim, R. Bai. Membrane fouling and cleaning in microfiltration of activated sludge wastewater. *Journal of Membrane Science*, 216 (2003), pp. 279-290.
- [21] Z. Wang, J. Chu, X. Zhang. Study of a cake model during stirred dead-end microfiltration. *Desalination*, 217 (2007), pp. 127-138.
- [22] S. Judd. Fundamentals. In: S. Judd (Ed.), *The MBR Book* (second edition), Butterworth-Heinemann, Oxford (2011), pp. 55-207.
- [23] V.V. Tarabara, I. Koyuncu, M.R. Wiesner. Effect of hydrodynamics and solution ionic strength on permeate flux in cross-flow filtration: direct experimental observation of filter cake cross-sections. *Journal of Membrane Science*, 241 (2004), pp. 65-78.
- [24] K.-J. Hwang, Y.-S. Wu, W.-M. Lu. The surface structure of cake formed by uniform-sized rigid spheroids in cake filtration. *Powder Technology*, 87 (1996), pp. 161-168.
- [25] L. Defrance, M.Y. Jaffrin, B. Gupta, P. Paullier, V. Geaugey. Contribution of various constituents of activated sludge to membrane bioreactor fouling. *Bioresource Technology*, 73 (2000), pp. 105-112.
- [26] H.H.P. Fang, X. Shi. Pore fouling of microfiltration membranes by activated sludge. *Journal of Membrane Science*, 264 (2005), pp. 161-166.
- [27] K.-H. Choo, C.-H. Lee. Membrane fouling mechanisms in the membrane-coupled anaerobic bioreactor. *Water Research*, 30 (1996), pp. 1771-1780.
- [28] W.-W. Li, Y.-K. Wang, J. Xu, Y.-R. Tong, L. Zhao, H. Peng, G.-P. Sheng, H.-Q. Yu. A dead-end filtration method to rapidly and quantitatively evaluate the fouling resistance of

- nylon mesh for membrane bioreactors. *Separation and Purification Technology*, 89 (2012), pp. 107-111.
- [29]G. Bolton, D. LaCasse, R. Kuriyel. Combined models of membrane fouling: development and application to microfiltration and ultrafiltration of biological fluids. *Journal of Membrane Science*, 277 (2006), pp. 75-84.
- [30]J.A. Suarez, J.M. Veza. Dead-end microfiltration as advanced treatment for wastewater. *Desalination*, 127 (2000), pp. 47-58.
- [31]C. Duclos-Orsello, W. Li, C.C. Ho. A three-mechanism model to describe fouling of microfiltration membranes. *Journal of Membrane Science*, 280 (2006), pp. 856-866.
- [32]T.C. Arnot, R.W. Field, A.B. Koltuniewicz. Cross-flow and dead-end microfiltration of oily-water emulsions: Part II. Mechanisms and modelling of flux decline. *Journal of Membrane Science*, 169 (2000), pp. 1-15.
- [33]S. Mondal, S. De. A fouling model for steady-state crossflow membrane filtration considering sequential intermediate pore blocking and cake formation. *Separation and Purification Technology*, 75 (2010), pp. 222-228.